RESEARCH BRIEF

SHP2 Inhibition Prevents Adaptive Resistance to MEK Inhibitors in Multiple Cancer Models

Carmine Fedele[1], Hao Ran[1], Brian Diskin[2], Wei Wei[1], Jayu Jen[1], Mitchell J. Geer[1], Kiyomi Araki[1], Ugur Ozerdem[3], Diane M. Simeone[1], George Miller[2], Benjamin G. Neel[1], and Kwan Ho Tang[1]

ABSTRACT Adaptive resistance to MEK inhibitors (MEKi) typically occurs via induction of genes for different receptor tyrosine kinases (RTK) and/or their ligands, even in tumors of the same histotype, making combination strategies challenging. SHP2 (*PTPN11*) is required for RAS/ERK pathway activation by most RTKs and might provide a common resistance node. We found that combining the SHP2 inhibitor SHP099 with a MEKi inhibited the proliferation of multiple cancer cell lines *in vitro*. *PTPN11* knockdown/MEKi treatment had similar effects, whereas expressing SHP099 binding–defective *PTPN11* mutants conferred resistance, demonstrating that SHP099 is on-target. SHP099/trametinib was highly efficacious in xenograft and/or genetically engineered models of *KRAS*-mutant pancreas, lung, and ovarian cancers and in wild-type RAS-expressing triple-negative breast cancer. SHP099 inhibited activation of KRAS mutants with residual GTPase activity, impeded SOS/RAS/MEK/ERK1/2 reactivation in response to MEKi, and blocked ERK1/2-dependent transcriptional programs. We conclude that SHP099/MEKi combinations could have therapeutic utility in multiple malignancies.

SIGNIFICANCE: MEK inhibitors show limited efficacy as single agents, in part because of the rapid development of adaptive resistance. We find that SHP2/MEK inhibitor combinations prevent adaptive resistance in multiple cancer models expressing mutant and wild-type KRAS. *Cancer Discov; 8(10); 1237–49. ©2018 AACR.*

See related commentary by Torres-Ayuso and Brognard, p. 1210.

INTRODUCTION

The RAS/ERK pathway is one of the most commonly affected signaling pathways in human cancer (1–3). Mutations in genes encoding pathway components, including those for receptor tyrosine kinases (RTK), SHP2, NF1, RAS, or RAF, cause inappropriate pathway activation and promote oncogenesis. Attempts have been made to target the ERK pathway in different cancer types and can lead to initial responses. Unfortunately, a form of intrinsic resistance termed "adaptive resistance" occurs frequently, resulting in lack of efficacy, recurrence, or progression (4).

[1]Laura and Isaac Perlmutter Cancer Center, New York University School of Medicine, NYU Langone Health, New York, New York. [2]S. Arthur Localio Laboratory, Department of Surgery, New York University School of Medicine, NYU Langone Health, New York, New York. [3]Department of Pathology, New York University School of Medicine, NYU Langone Health, New York, New York.

Note: Supplementary data for this article are available at Cancer Discovery Online (http://cancerdiscovery.aacrjournals.org/).

Corresponding Authors: Benjamin G. Neel, New York University School of Medicine, 522 First Avenue, Smilow Building 12th Floor, Suite 1201, New York, NY 10016. Phone: 212-263-3019; Fax: 212-263-9190; E-mail: Benjamin.Neel@nyumc.org; Kwan Ho Tang, KwanHo.Tang@nyumc.org; and Carmine Fedele, Carmine.Fedele@nyumc.org

doi: 10.1158/2159-8290.CD-18-0444

KRAS is the most frequently mutated RAS/ERK pathway gene (1–3). Approaches to target *KRAS*-mutant cancers with MEK inhibitors (MEKi) have failed, often due to the induction of RTK genes and/or their ligands. For example, FGFR1 is activated in MEKi-treated *KRAS*-mutant lung cancers, leading to increased upstream signaling and ERK reactivation (5). Another group found that MEKi resistance can be mediated through ERBB3 in *KRAS*-mutant lung and colon cancers (6), whereas a third reported that MEKi treatment leads to EGFR activation in *KRAS*-mutant pancreatic cancer lines (7). Malignancies that lack mutations in pathway genes but nonetheless hyperactivate ERK also show adaptive resistance in response to MEKi. For example, MEKi-treated triple-negative breast cancer (TNBC) cells induce the expression of genes encoding AXL, DDR1, FGFR2, IGF1R, KIT, PDGFRB, and VEGFRB (8, 9).

Because resistance to MEKi can be mediated by multiple RTKs, combining MEK and RTK inhibition is probably not a viable therapeutic approach. However, a strategy that efficiently blocks signals from multiple activated RTKs might prevent adaptive resistance. The protein-tyrosine phosphatase SHP2 is a positive (i.e., signal-enhancing) signal transducer, acting between RTKs and RAS (10, 11). A potent, highly specific inhibitor targeting SHP2, SHP099, has been developed and blocks ERK activation and proliferation of cancer cells driven by overexpressed, hyperactivated RTKs (12, 13). We hypothesized that SHP099 would inhibit signals from RTKs activated following MEK inhibition and thereby block adaptive resistance. This idea comports with the previous finding that *PTPN11* shRNA or CRISPR/Cas9-mediated deletion prevents adaptive resistance to vemurafenib in *BRAF*-mutant colon cancer (14).

Here, we test this hypothesis in multiple *KRAS*-mutant and wild-type (WT) cancer cells from different histotypes. Our results suggest that SHP2 inhibition could provide a general strategy for preventing MEKi resistance in a wide range of malignancies and might also have single-agent efficacy against KRAS mutants that retain significant GTPase activity.

RESULTS

SHP099 Abrogates Adaptive Resistance to MEKi *In Vitro*

Previous work showed that several cancer models develop adaptive resistance to MEKi through RTK upregulation. We analyzed RTK/RTK ligand gene expression by qRT-PCR in pancreatic ductal adenocarcinoma (PDAC) cell lines treated with AZD6244, a well-established MEKi (Fig. 1A). Consistent with earlier findings, several—but different—RTKs were induced by MEKi treatment, including *EGFR, FGFR3, IGFR1, MET,* and *PDGFRB* in MIAPaCa-2 cells, *ERBB2/3, FGFR2/3,* and *IGFR1* in Capan-2 cells, and *ERBB2/3* and *FGFR3* in CFPAC-1 cells. The same lines variably induced *EGF, FGF2, PDGFB, PDGFC, PDGFD,* and/or *VEGFA/B*. These observations make it difficult, if not impossible, to design an efficient combination therapy with MEKi by targeting RTKs directly.

To explore whether SHP2 inhibition could suppress MEKi adaptive resistance, we performed *in vitro* viability (PrestoBlue) and colony formation assays on a panel of *KRAS*-mutant PDAC lines (Fig. 1B and C). Resistant cell populations and drug-resistant colonies were observed after 7 or 10 days, respectively, of AZD6244 treatment. AZD6244 itself had variable effects, leading to 30% to 90% reduction in proliferation/colony formation compared with control DMSO treatment; nevertheless, nearly all lines showed significant resistance. Consistent with a previous report (12), *KRAS*-mutant cell lines exhibited low sensitivity to SHP099 alone. By contrast, all but two of the lines had markedly reduced cell numbers and few or no detectable colonies after SHP099/MEKi combination treatment; in most cases, the combination was synergistic (Fig. 1B, red asterisks; Supplementary Table S1). Similar effects were seen in growth curve assays (Supplementary Fig. S1A), with the more potent MEKi trametinib (Supplementary Fig. S1B), and on short-term cultures of cells from patient-derived xenografts (PDX) and in *KRAS*-mutant non–small cell lung cancer (NSCLC) lines (Supplementary Fig. S1C–S1E). The drug combination decreased cell-cycle progression and, in some lines, enhanced cell death (measured at 48 hours and 6 days of treatment, respectively), compared with either single agent alone (Supplementary Fig. S1F).

Expression of a mutant (*PTPN11*^{P491Q}) predicted to lack SHP099 binding in MIAPaCa-2 cells (which are quite sensitive to SHP099/MEKi) and in KPC 1203, a cell line derived from induced *LSL-KRAS*^{G12D}*Trp53*^{R172H} (KPC) mice (15), eliminated the effects of SHP099 in combination-treated cells (Fig. 1D and E). Another drug-resistant mutant, *PTPN11*$^{T253M/Q257L}$ (12), rescued the effects of the combination on H358 NSCLC cells (Fig. 1D). Moreover, combining MEK inhibition and *PTPN11* shRNA expression had similar effects to SHP099/MEKi treatment (Fig. 1F). These data indicate that SHP099 is "on-target" and that SHP2 inhibition diminishes adaptive resistance to MEKi in multiple *KRAS*-mutant cancer cell lines, arising from two distinct tissues.

Figure 1. Combined SHP2 and MEK inhibition abrogates adaptive resistance in PDAC cell lines. **A,** Time-dependent increase in RTK (left) and RTK ligand (right) gene expression in PDAC cells after DMSO, SHP099, AZD6244, or SHP099/AZD6244 (Combo) treatment, determined by qRT-PCR. **B** and **C,** PDAC cell lines were treated with DMSO, SHP099, AZD6244, or both drugs (Combo). Cell viability, by PrestoBlue assay (**B**), and colony formation (**C**) were assessed at 7 or 10 days, respectively. *, $P < 0.05$; **, $P < 0.01$; ***, $P < 0.001$, two-tailed *t* test. Representative results from a minimum of three biological replicates are shown per condition. Red asterisks indicate synergistic interaction between the two drugs by BLISS independent analysis. **D,** Colony formation assay (1 week) in MIAPaCa-2 cells either expressing an SHP099-resistant *PTPN11* mutant (P491Q) or wild-type *PTPN11* (WT) and H358 NSCLC cells expressing an SHP099-resistant *PTPN11* mutant (T253M/Q257L) or wild-type *PTPN11* (WT). ***, $P < 0.001$, two-sided *t* test. **E,** Colony formation assay (1 week) in KPC 1203 cells either expressing an SHP099-resistant *PTPN11* mutant (P491Q) or wild-type *PTPN11* (WT). **F,** Colony formation assay (1 week) in MIAPaCa-2 (left) and (10 days) Panc 03.27 (right) cells expressing IPTG-inducible *PTPN11* (shSHP2) or CTRL (shGFP) shRNAs. Representative results from a minimum of three biological replicates are shown per condition. For all experiments, drug doses were: SHP099 10 μmol/L, AZD6244 1 μmol/L, Combo = SHP099 10 μmol/L + AZD6244 1 μmol/L. Trametinib (10 nmol/L) was used where indicated.

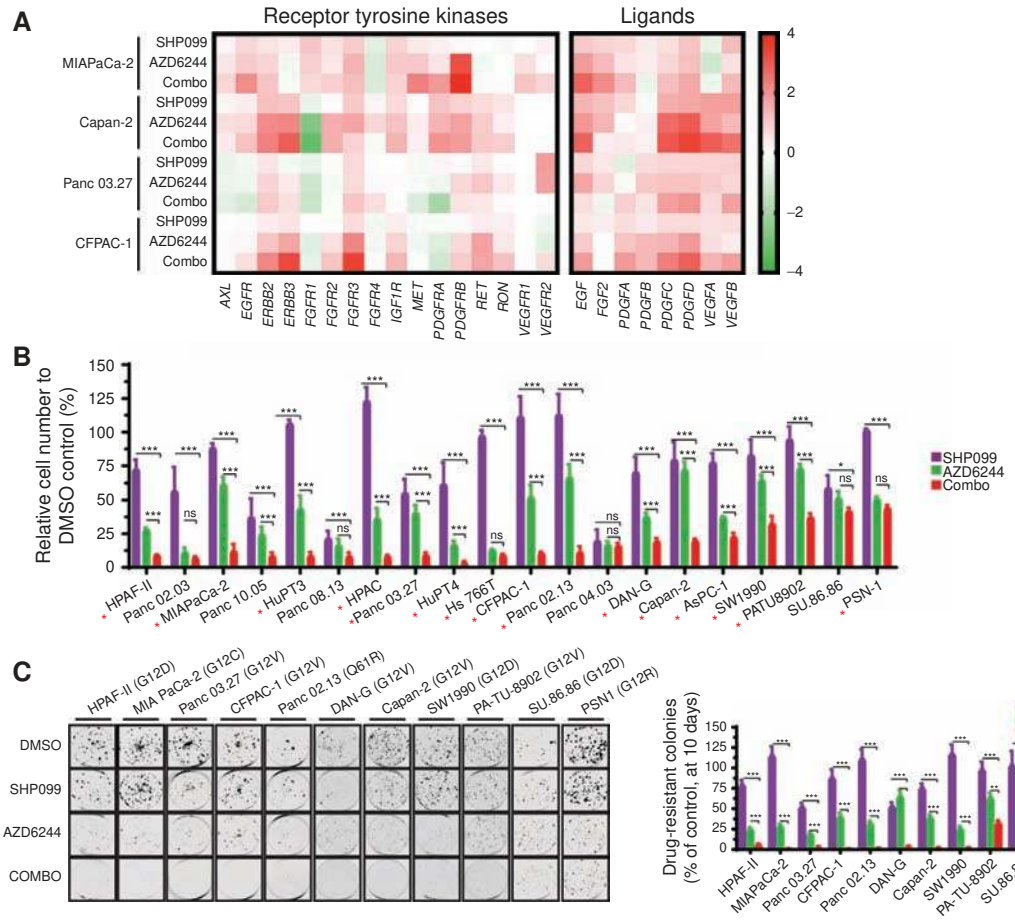

SHP099 Impedes MEKi–Induced Reactivation of the MAPK Pathway

We assessed the biochemical effects of each single agent and the drug combination on RAS/ERK pathway activity after short-term (1 hour) and longer-term (48 hours) treatments. Short-term AZD6244 exposure had no detectable effect on RAS. At 48 hours, however, RAS activation (monitored by RAF-RBD assay) was enhanced, consistent with signaling from the induced RTKs/RTK ligands (Fig. 2A). Isoform-specific antibodies revealed increased activation of KRAS and NRAS in response to 48 hours MEKi treatment of MIAPaCa-2 cells (Fig. 2B). SHP2 acts upstream of RAS, but whether it promotes RAS exchange (e.g., via SOS), inhibits RAS-GAP, or both, has been less clear (10, 11). MIAPaCa-2 cells have no WT KRAS (mutant allele frequency = 0.99; refs. 16, 17), so the increase in KRAS activation following MEKi treatment must reflect enhanced cycling of $KRAS^{G12C}$. As $KRAS^{G12C}$ is highly resistant to RAS-GAP (18), the decreased KRAS-GTP in SHP099/AZD6244-treated MIAPaCa-2 cells indicates that residual $KRAS^{G12C}$ GTPase activity contributes significantly to the steady-state level of KRAS-GTP in these cells and that SHP2 must promote RAS exchange. Increased NRAS-GTP in response to SHP099 reflects activation of normal, endogenous NRAS.

The other PDAC lines tested express KRAS mutants with less intrinsic GTPase activity than $KRAS^{G12C}$ (18) and retain WT KRAS. Hence, it was not clear whether SHP099 can also block activation of these RAS mutants in response to MEKi treatment or affects WT KRAS or the other RAS isoforms (Fig. 2A). To more directly interrogate the effects of SHP2 inhibition on other KRAS mutants, we used RAS-less mouse embryonic fibroblasts (MEF; ref. 19). As in MIAPaCa-2 cells, $KRAS^{G12C}$-reconstituted RAS-less cells showed increased KRAS-GTP after 48 hours of MEKi treatment, and this increase was prevented by SHP099. By contrast, SHP099 had no effect on $KRAS^{Q61R}$-GTP levels (Fig. 2C). The ability of single-agent SHP099 to inhibit ERK activation in RAS-less MEFs reconstituted with different KRAS mutants was linearly related to their reported GTPase activities (ref. 17; Fig. 2D). These results confirm that SHP2 is required for RAS exchange, most likely acting upstream of SOS1/2. Indeed, expressing the SOS1 catalytic domain tagged with a C-terminal CAAX BOX of RAS (20) rescued the effects of SHP099 on ERK activation in MIAPaCa-2 cells (Fig. 2E).

Single-agent AZD6244 blocked MEK activity and ERK1/2 phosphorylation after 1 hour, but these effects were successively abolished after 24 and 48 hours of treatment, respectively, and MEK and ERK activity rebounded (Fig. 2F; Supplementary Fig. S2A). Trametinib also caused MEK/ERK rebound, although to a lesser extent (Supplementary Fig. S2B). Consistent with its effects on RAS, SHP099 coadministration blocked the adaptive increase in MEK and ERK phosphorylation in response to either MEKi (Fig. 2F; Supplementary Fig. S2A and S2B). ERK-dependent gene expression can provide a more sensitive assessment of pathway output than phospho-ERK (pERK) levels (21), so we measured FOS-like 1 (*FOSL1*) and ETS variants 1, 4, 5 (*ETV1, 4,* and *5*) RNA by qRT-PCR. Compared with the effects of either single agent, the SHP099/AZD6244 or SHP099/trametinib combination caused greater suppression of ERK-dependent transcription (Fig. 2G; Supplementary Fig. S2C). Other RTK-evoked pathways (e.g., PI3K/AKT, STAT, and JNK/p38) showed no consistent effects of either single agent or the drug combination (Supplementary Fig. S2D and data not shown). These findings confirm that ERK reactivation is a key component of the adaptive program activated in *KRAS*-mutant cancer cells treated with MEKi and show that SHP099 blocks this adaptive response. Importantly, the biochemical effects of SHP099 (like its effects on colony formation; Fig. 1D) were reversed in MIAPaCa-2 (Fig. 2H), H358 (Supplementary Fig. S2E), and KPC 1203 cells expressing SHP099-resistant SHP2. *PTPN11* depletion had similar biochemical effects as SHP2 inhibition (Fig. 2J), confirming on-target effects of SHP099.

We also explored the mechanism of resistance of two *KRAS*-mutant PDAC lines to SHP099/MEKi. PSN1 cells failed to suppress MEK–ERK reactivation or ERK-dependent gene expression (Supplementary Fig. S3A and S3B). In SU.86.86 cells, MEK/ERK and ERK-dependent genes were inhibited to an extent similar to sensitive cells, consistent with a downstream escape mechanism (Supplementary Fig. S3C and S3D). Further investigation will be required to uncover the precise molecular explanation for resistance in these cell lines.

Combined SHP2/MEK Inhibition Suppresses *KRAS*-Mutant Tumor Growth *In Vivo*

We next established Capan-2, MIAPaCa-2, and H358 xenografts and treated them with vehicle control (methyl-

Figure 2. SHP2 inhibition acts upstream of RAS to abrogate MEKi–evoked ERK MAPK pathway reactivation. **A** and **B,** Immunoblots of whole-cell lysates or GST-RBD–precipitated (RAS-GTP, KRAS-GTP, and NRAS-GTP) lysates from PDAC cells treated with DMSO, SHP099 (10 μmol/L), AZD6244 (1 μmol/L), or both drugs for the times indicated. The images shown are representative of at least two independent biological replicates. **C,** GST-RBD pulldown assay on RAS-less MEFs reconstituted with RAS^{G12C} or RAS^{Q61R}. Total RAS, pERK/ERK, and pMEK/MEK were also detected in whole-cell lysates prepared in modified RIPA buffer from the same cells. **D,** Immunoblots of whole-cell lysates from RAS-less MEFs reconstituted with $KRAS^{WT}$, $KRAS^{G12C}$, $KRAS^{G12D}$, or $KRAS^{Q61R}$, treated with or without 10 μmol/L SHP099 (left). Linear regression of SHP099-induced pERK inhibition compared with intrinsic GTPase activity of the different KRAS mutants (from ref. 17) in RAS-less MEFs (right). **E,** Effect of SHP099 on pERK levels in MIAPaCa-2 cells expressing a SOS1 mutant (SOS B1) that targets the SOS1 catalytic domain constitutively to the plasma membrane. Cells were incubated for 1 hour with SHP099, and lysates were immunoblotted for pERK and total ERK (as a loading control). **F,** Immunoblots of lysates from PDAC lines treated as indicated. The image shown is representative of three independent biological replicates. **G,** ERK-dependent gene expression (*ETV1, 4, 5* and *FOSL1*), assessed by qRT-PCR, in PDAC lines treated as indicated (*, $P < 0.05$; **, $P < 0.01$; ***, $P < 0.001$; ****, $P < 0.0001$, two-tailed *t* test). **H,** Immunoblots of SHP2, pERK, ERK, pMEK, and MEK from MIAPaCa-2 cells ectopically expressing wild-type SHP2 (WT) or an SHP099-resistant mutant (P491Q), treated as indicated. **I,** ERK-dependent gene expression in MIAPaCa-2 cells ectopically expressing wild-type SHP2 (WT) or an SHP099-resistant mutant (P491Q), treated as in **F** (*, $P < 0.05$; **, $P < 0.01$; ***, $P < 0.001$; ****, $P < 0.001$, two-tailed *t* test). **J,** Immunoblot of lysates from MIAPaCa-2 (top) and Panc 03.27 (bottom) cells expressing IPTG-inducible *PTPN11* (shSHP2) or CTRL (shGFP) shRNA, subjected to the indicated drugs. Numbers under blots indicate relative intensities, compared with untreated controls, quantified by LI-COR.

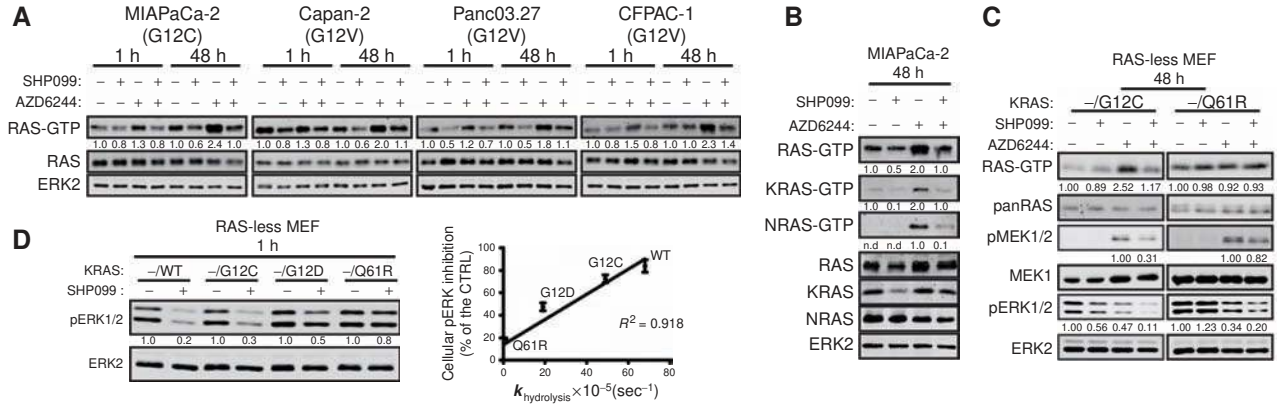

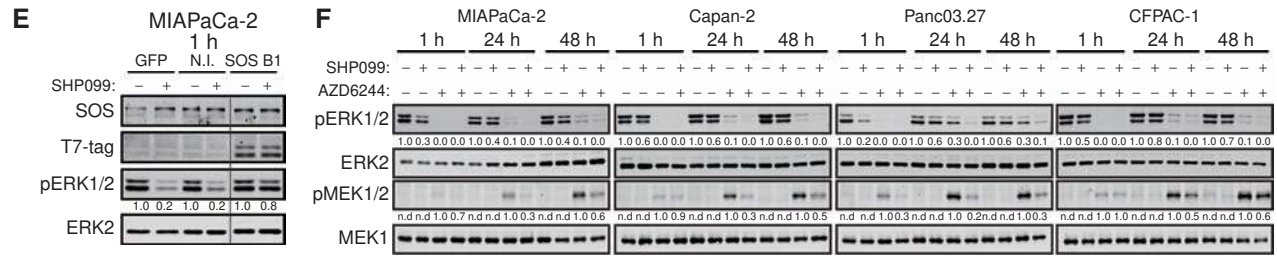

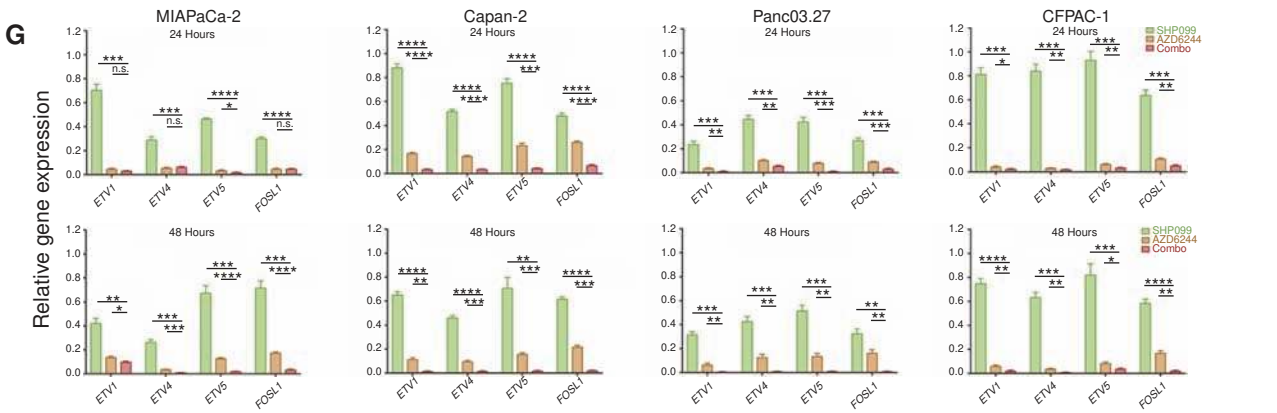

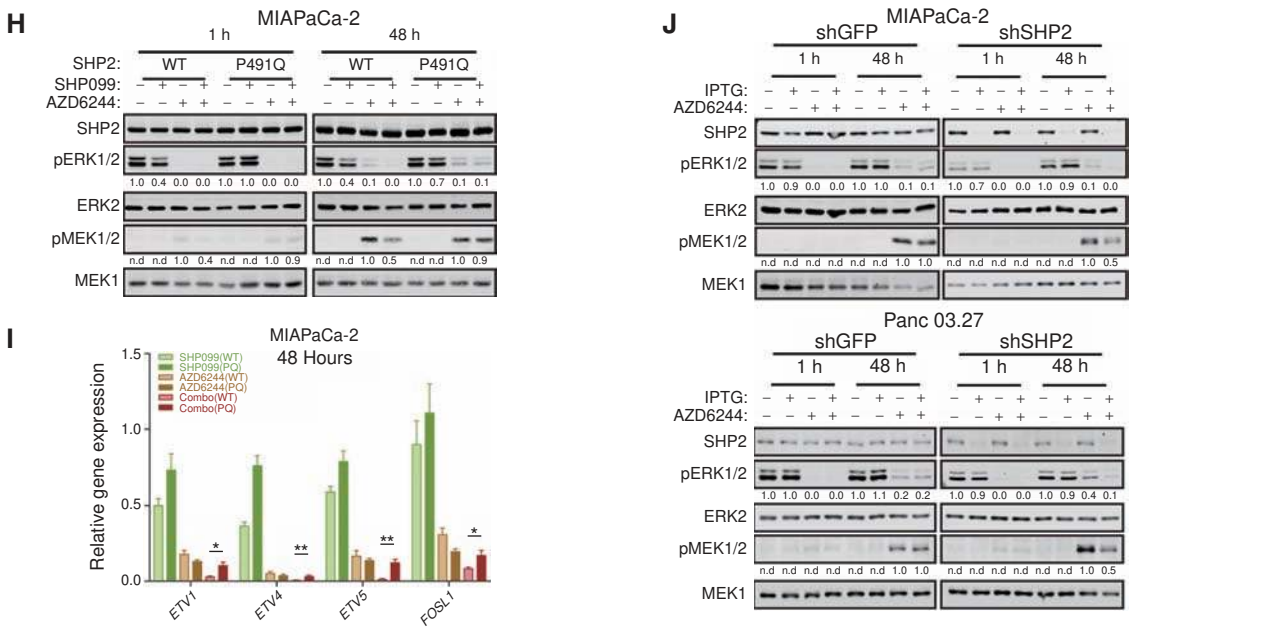

cellulose+Tween80), trametinib alone, SHP099 alone, or SHP099/trametinib. We used trametinib because of its favorable mouse pharmacokinetic properties ($t_{½}$ = 33 hours; ref. 22), which enable single daily dosing, as does SHP099 (13). In initial experiments, mice were treated daily with trametinib (1 mg/kg), a dose used commonly in mouse tumor studies (6, 23, 24), SHP099 (75 mg/kg), or both. Each single agent was well tolerated, but mice receiving the combination lost weight (>10%), exhibited lassitude, and began dying at day 7 of treatment. Some showed gross gastrointestinal (GI) bleeding (Supplementary Fig. S4A), and histology revealed multifocal GI tract ulceration, acute esophagitis and gastritis, and villus blunting, which could explain malabsorption, diarrhea, and weight loss (Supplementary Fig. S4B).

Although trametinib is usually administered to mice at this dose or even at doses as high as 3 mg/kg (5, 25), the mouse allometric equivalent of the maximum tolerated dose (MTD) in humans is ~0.25 mg/kg (26). We treated a small group of mice with this dose of trametinib and SHP099 (75 mg/kg) daily (q.d.). Although treated mice lived longer than with the higher trametinib dose, this combination also led to weight loss and death (data not shown). Exploratory dose finding resulted in a tolerable schedule, in which trametinib is delivered at 0.25 mg/kg, with SHP099 (75 mg/kg) every other day (q.o.d.). These mice showed no observable histopathology (Supplementary Fig. S4C). A few developed mild, self-limited, non-bloody diarrhea, but all showed stable weight and normal behavior and appeared healthy for up to 37 days of continuous treatment (Supplementary Fig. S4D and S4E and data not shown).

Capan-2, MIAPaCa-2, or H358 xenografts were allowed to grow to 500 mm^3 (Fig. 3A), and then mice were treated with vehicle, trametinib (0.25 mg/kg q.d.), SHP099 (75 mg/kg q.d.), or trametinib (0.25 mg/kg q.d.)/SHP099 (75 mg/kg q.o.d.). Remarkably, the combination caused substantial regressions in all mice (Fig. 3A; Supplementary Fig. S4F). Tumor shrinkage averaged >65% in the three models, well above RECIST criteria (27). The decrease in tumor size probably underestimates the antineoplastic effect, as the ratio of tumor cells/area also decreased, with the residual area occupied by fibroblasts (Fig. 3B and C). Strikingly, Capan-2 xenografts treated for 37 days with SHP099/trametinib failed to regrow after 40 days of drug withdrawal (Fig. 3D). The residual tumor appeared to have undergone cellular senescence, as shown by βgal staining (Fig. 3E) and elevated expression of the senescence-associated cytokine IL6 (Fig. 3F).

Single-agent effects were more variable both within each treatment group and in mice bearing MIAPaCa-2 versus Capan-2/H358–derived tumors. Trametinib had minimal effects on MIAPaCa-2 tumors, although it caused significant shrinkage of about half of the Capan-2 and H358 xenografts (Fig. 3A; Supplementary Fig. S4F). Only a few trametinib-treated mice met RECIST criteria (>30%), however, and the SHP099/MEKi combination was more effective (Fig. 3A; Supplementary Fig. S4F). Surprisingly, in contrast to its lack of effect on proliferation in cell culture or on colony formation, SHP099 alone caused tumor shrinkage in ~80% of Capan-2, ~60% of MIAPaCa-2, and ~70% of H358 xenografts. It is not clear whether this discrepancy reflects effects of SHP099 on normal RAS/ERK signaling in cells within the tumor microenvironment (e.g., fibroblasts and blood vessels), effects on the malignant cells themselves with secondary consequences for stroma, or both. Consistent with at least some nonautonomous effects, SHP099 decreased tumor vascularity as monitored by CD31 immunostaining (Fig. 3B and C), without major effects on VEGF or FGF mRNA levels (see Fig. 3J). Nevertheless, single-agent SHP099 was, like trametinib alone, inferior to the drug combination (Fig. 3A; Supplementary Fig. S4F). Comporting with these biological effects, immunoblotting (Fig. 3G; Supplementary Fig. S4G), qRT-PCR (Fig. 3H), and IHC analysis (Fig. 3I) revealed greater pERK inhibition in combination- than in single agent–treated tumors. Notably, tumors induced RTK and RTK ligand expression following MEKi treatment, confirming that adaptive resistance via RTK overactivation occurs *in vivo* (Fig. 3J).

We also tested syngeneic mice injected orthotopically with KPC 1203 cells. Tumors were allowed to grow for 10 days, 5 mice were sacrificed to obtain baseline tumor sizes, and the rest were treated with single agent or SHP099/trametinib for 5 or 15 days, respectively. Again, mice in the combination arms showed markedly inhibited tumor growth, compared with trametinib-treated mice (Fig. 3K and L). Although the combination was superior (day 15; Fig. 3L), SHP099 also had significant effects, even though $KRAS^{G12D}$ has significantly less residual GTPase activity than $KRAS^{G12C}$ (18). Immunoblot analysis revealed greater inhibition of pERK and DUSP6 (an ERK target gene product) in combination-treated tumors than in those treated with trametinib or SHP099 alone (Fig. 3M).

As in the xenografts, tumor vascularity and overall tumor cellularity was reduced in combination-treated genetically engineered mouse models (GEMM; Fig. 3N and O). Furthermore, residual tumor cells in combination-treated mice showed ductal differentiation, compared with vehicle- or single agent–treated mice (Fig. 3P). PAS/Alcian Blue staining revealed secretory activity (Fig. 3P), whereas qRT-PCR analysis showed induction of ductal and, more prominently, endocrine markers (Supplementary Fig. S4H). All SHP099/trametinib-treated xenografts and syngeneic tumors showed decreased proliferation and increased apoptotic cell death (Supplementary Figs. S5 and S6).

SHP099/MEKi Combination Is Also Effective in TNBC and Serous Ovarian Cancer Models

Genetic (28, 29) and functional genomic (30, 31) analyses reveal striking similarities between TNBC and high-grade serous ovarian cancer (HGSC). These malignancies typically express WT RAS, and in some TNBC models MEK inhibition results in RTK upregulation and adaptive resistance (8). To explore the potential generality of combination MEK/SHP2 inhibition as a therapeutic strategy (and the utility of this combination in adaptive resistance to MEKi in WT RAS–expressing cells), we tested SHP099/MEKi combinations in TNBC and HGSC models.

Similar to its effects on *KRAS*-mutant cells, MEKi treatment increased RTK and RTK ligand gene expression in TNBC and HGSC lines (Supplementary Fig. S7A). SHP099 (10 μmol/L) alone had little effect on cell number or colony

formation (Fig. 4A and B; Supplementary Fig. S7B). The MEKi AZD6244 or UO126 had variable single-agent effects, often (but not always) causing reduced cell proliferation compared with controls. Nevertheless, resistant cell populations were seen in almost all cell lines. The SHP099/MEKi combination showed increased efficacy, with additive to synergistic effects (Fig. 4A; Supplementary Fig. S7B; Supplementary Table S1). As in *KRAS*-mutant cell models (above), combination treatment slowed cell-cycle progression and enhanced cell death (Supplementary Fig. S7C and S7D). After 48 hours of single-agent treatment, SHP099 had little or no effect on RAS activation in any of the models

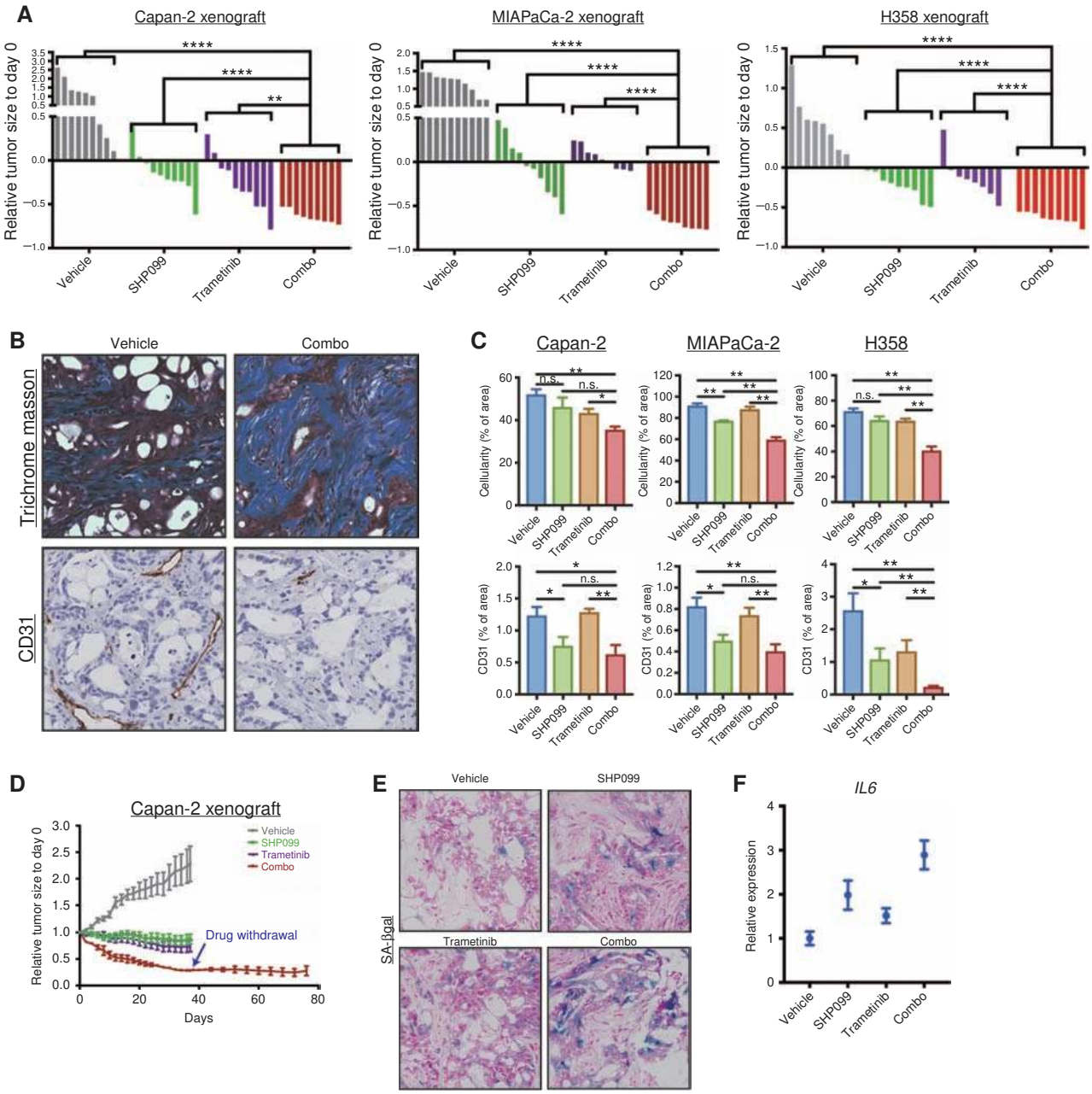

Figure 3. Combined MEK/SHP2 inhibition is efficacious in PDAC models *in vivo*. **A,** Response of Capan-2, MIAPaCa-2, and H358 subcutaneous xenografts to treatment with SHP099 (75 mg/kg body weight, q.d.), trametinib (0.25 mg/kg q.d.) or both drugs (trametinib 0.25 mg/kg q.d.; SHP099 75 mg/kg q.o.d.). Waterfall plot shows response of each tumor after 37 days (Capan-2), 19 days (MIAPaCa-2), and 21 days (H358) of treatment; $n = 8$–10 mice per group (*, $P < 0.05$; **, $P < 0.01$; ***, $P < 0.001$; ****, $P < 0.0001$, two-tailed Mann–Whitney test). **B,** Masson Trichrome (collagen) and CD31 (blood vessels) staining in treated Capan-2 tumors showing reduced tumor cellularity and vascularity, respectively. **C,** Quantification of tumor cellularity (Masson Trichrome stain) and vascularity (CD31) of treated Capan-2, MIAPaCa-2, and H358 xenografts (*, $P < 0.05$; **, $P < 0.01$; ***, $P < 0.001$; ****, $P < 0.0001$, Masson Trichrome: two-tailed *t* test, CD31: one-tailed *t* test). **D,** Tumor growth curve of treated Capan-2 xenografts (drug withdrawal after 37 days of combo treatment). **E,** SA-β gal staining on treated Capan-2 tumors following 37 days of treatment. **F,** qRT-PCR of senescence-associated cytokine *IL6* in treated Capan-2 tumors. (*continued on next page*)

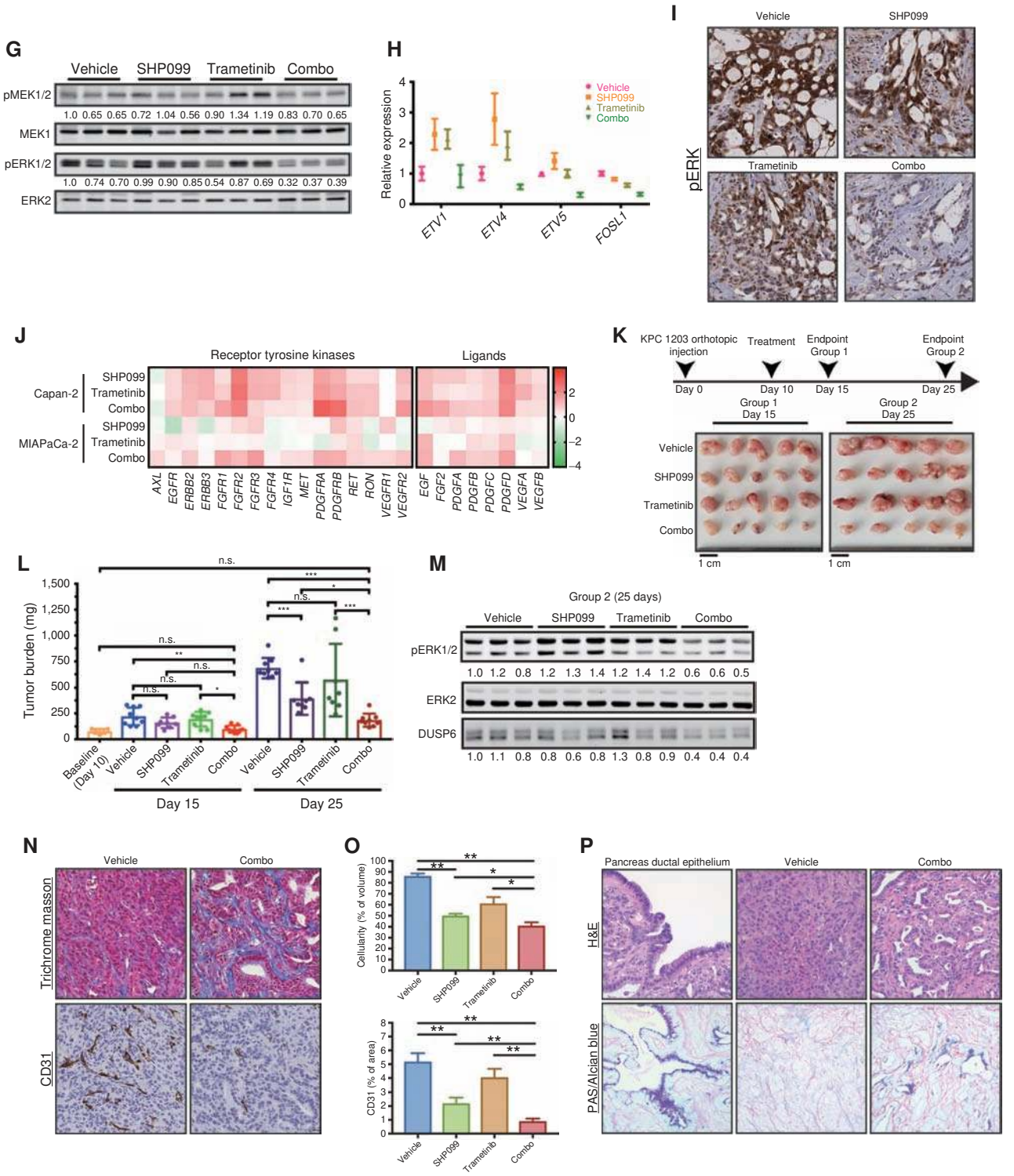

Figure 3. ***(Continued)*** **G,** Immunoblot showing pERK and pMEK levels in treated Capan-2 tumors. **H,** ERK-dependent gene expression (*ETV1, 4, 5* and *FOSL1*), assessed by qRT-PCR, in Capan-2 tumors. **I,** Immunohistochemical stain for pERK in treated Capan-2 tumors. **J,** qRT-PCR of RTK and RTK ligand genes in treated Capan-2 and MIAPaCa-2 tumors. **K** and **L,** Syngeneic mice injected orthotopically with KPC 1203 cells were treated with vehicle, SHP099 (75 mg/kg q.d.), trametinib (0.25 mg/kg q.d.), or both drugs (trametinib 0.25 mg/kg q.d.; SHP099 75 mg/kg q.o.d.), as depicted in the scheme. Tumor mass was measured at days 15 and 25 (*, $P < 0.05$; **, $P < 0.01$; ***, $P < 0.001$, one-way ANOVA with Tukey multiple comparison test). **M,** Immunoblot showing pERK and DUSP6 levels in KPC 1203 tumors from **K**. **N** and **O,** Masson Trichrome and CD31 staining and quantification in treated KPC tumors. **P,** Hematoxylin and eosin (H&E) and PAS/Alcian Blue staining of treated KPC tumors. Numbers under blots indicate relative intensities, compared with untreated controls, quantified by LI-COR.

(Fig. 4D). After MEKi treatment, however, RAS was hyperactivated to varying degrees in MDA-MB-468, HCC1954, CAL-120, and OVCAR-8 cells. In SHP099/MEKi–treated cells, RAS-GTP decreased to normal levels in randomly growing cells. These findings indicate that RAS activation is largely SHP2-independent under normal serum growth conditions, but is essential for the increase in RAS-GTP caused by the adaptive (RTK-driven) program evoked by MEKi treatment. As expected, 48-hour AZD6244 treatment led to increased MEK1/2 and ERK phosphorylation; consistent with its effects on RAS, SHP099 suppressed this increase (Fig. 4E), as well as ERK-dependent gene expression (Fig. 4F).

Finally, we treated mice bearing mammary fat pad xenografts derived from MDA-MB-468 or an extremely aggressive HGSC PDX with SHP099, trametinib, or both drugs. Single agents did not produce consistent regressions of MDA-MB-468 xenografts, and the ovarian PDX was highly resistant to both drugs. However, SHP099/trametinib caused substantial regression of MDA-MB-468 xenografts and markedly inhibited the growth of the HGSC PDX (Fig. 4G and H; Supplementary Fig. S4F), while significantly reducing tumor angiogenesis and cellularity in both models (Fig. 4I). Decreased tumor cell proliferation and increased apoptosis were observed in combination-treated tumors (Supplementary Fig. S6).

DISCUSSION

Tumors evade targeted cancer therapies via an extensive repertoire of resistance mechanisms. One common theme involves activation of RTKs by inducing their expression and/or the expression of their ligands, which reactivates the inhibited pathway (5–9, 24, 32). Indeed, multiple, distinct sets of RTKs/RTK ligands were activated in response to MEKi treatment in the models that we tested. The heterogeneity of this adaptive response renders unfeasible combination therapies with MEKi and RTK inhibitors. However, targeting a common downstream component of RTK signaling in combination with MEKi might yield substantial efficacy. SHP2 has

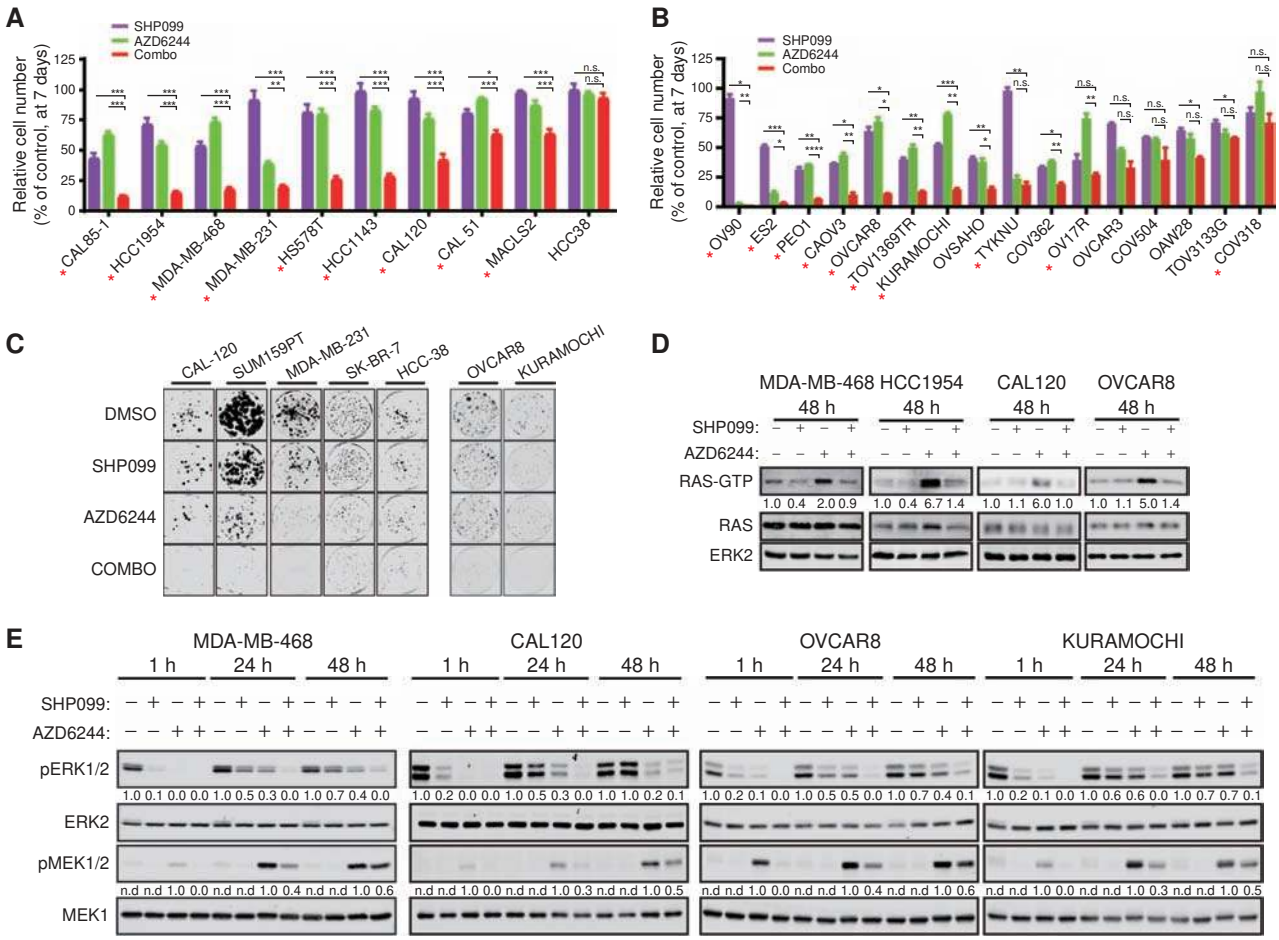

Figure 4. Combined MEK/SHP2 inhibition is also effective in TNBC and HGSC models. **A–C,** TNBC (**A**) and HGSC (**B**) cell lines were treated with DMSO, SHP099, AZD6244, or both (Combo). PrestoBlue intensity (**A**) or cell number (**B**) were assessed at 1 week. Colony formation (**C**) was quantified at 2 weeks. Representative results from a minimum of three biological replicates are shown per condition: SHP099 10 μmol/L, AZD6244 1 μmol/L, Combo = SHP099 10 μmol/L + AZD6244 1 μmol/L (*, $P < 0.05$; **, $P < 0.01$; ***, $P < 0.001$, two-tailed t test). Red asterisks indicate synergistic interaction between the two drugs by BLISS independent analysis. **D,** GST-RBD pulldown assay from TNBC and HGSC cell line lysates treated with DMSO, SHP099 10 μmol/L, AZD6244 1 μmol/L, or both for 48 hours. The image is representative of at least two independent experiments. **E,** Immunoblots of lysates from TNBC and HGSC lines, treated as indicated. The image is representative of three independent experiments. (*continued on next page*)

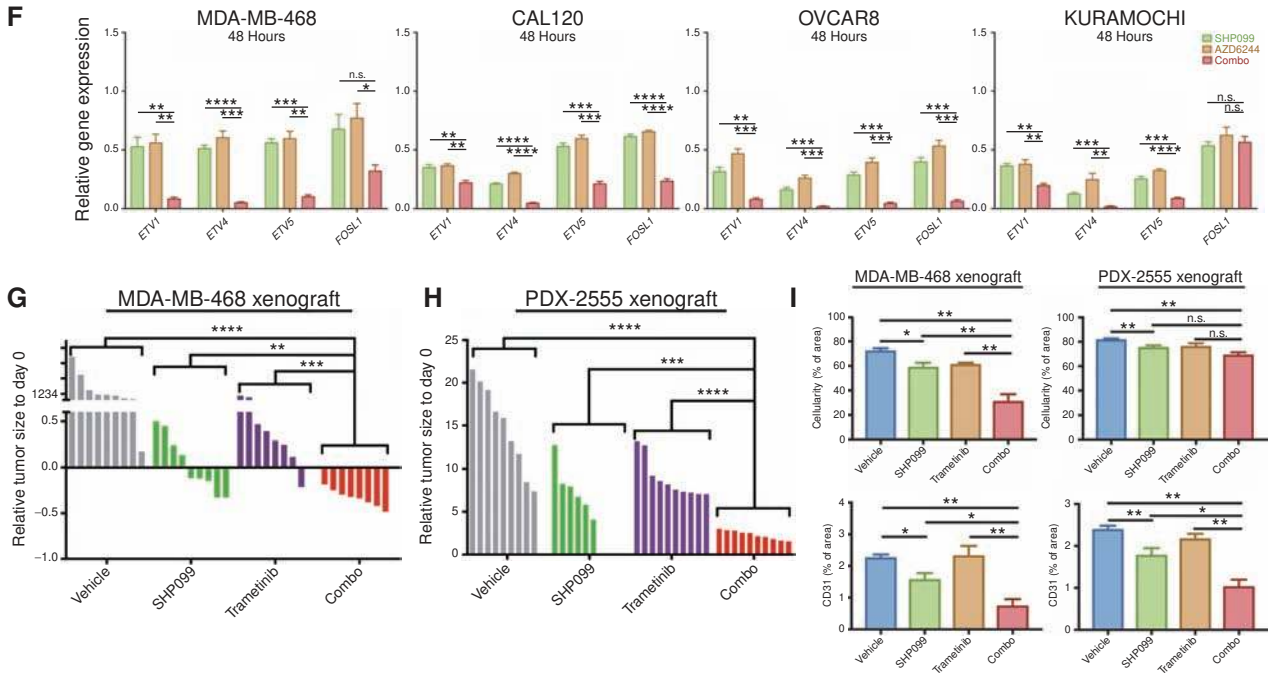

Figure 4. ***(Continued)*** **F,** ERK-dependent gene expression (*ETV1, 4, 5* and *FOSL1*), assessed by qRT-PCR, in TNBC and HGSC lines treated for 48 hours with the indicated drugs (*, $P < 0.05$; **, $P < 0.01$; ***, $P < 0.001$; ****, $P < 0.0001$, two-tailed *t* test). **G** and **H,** MDA-MB-468 (**G**) and PDX-2555 (**H**) mammary fat pad xenografts following treatment with SHP099 (75 mg/kg q.d.), trametinib (0.25 mg/kg q.d.), or both (trametinib 0.25 mg/kg q.d.; SHP099 75 mg/kg q.o.d.). Waterfall plots of tumor response after 29 days (MDA-MB-468) and 9 days (PDX-2555) of treatment are shown; $n = 8$–10 mice per group (*, $P < 0.05$; **, $P < 0.01$; ***, $P < 0.001$; ****, $P < 0.0001$, two-tailed Mann–Whitney test). **I,** Quantification of Masson Trichrome and CD31 staining of treated MDA-MB-468 and PDX-2555 tumor sections (*, $P < 0.05$; **, $P < 0.01$; ***, $P < 0.001$; ****, $P < 0.0001$, Masson Trichrome: two-tailed *t* test, CD31: one-tailed *t* test). Numbers under blots indicate relative intensities, compared with untreated controls, quantified by LI-COR.

long been known to signal downstream of normal RTKs (10, 11), and cancer cells dependent on RTK activity are susceptible to SHP099 monotherapy (12, 13). We find that combined MEK/SHP2 inhibition blocks cell proliferation and promotes shrinkage of tumors with increased RAS/ERK pathway activation, including those that typically have WT RAS (TNBC and HGSC), as well as those driven by mutant KRAS (PDAC and NSCLC). Unexpectedly, our studies also shed new light on the long-elusive effect of SHP2 on RAS.

Although SHP099 reportedly has off-target effects in some cells (33), it is clearly "on target" in our experiments. We observed its expected biochemical effects on RAS/ERK pathway activation in the multiple lines tested. Moreover, two different drug-resistant mutants (*PTPN11*^{P491Q} and *PTPN11*$^{T253M/Q257L}$) rescue the effects of SHP099 in PDAC and NSCLC cells, respectively, whereas *PTPN11* shRNA expression has similar biological and biochemical effects to SHP099. The MEKi used here also are highly validated, giving us confidence that the effects we observed reflect dual SHP2/MEK inhibition.

We expected SHP099 to block the adaptive increase in normal RAS activation that accompanies increased RTK signaling in MEKi–treated cells. Surprisingly, SHP099 also decreased mutant KRAS activation in MIAPaCA-2 cells, which only express KRAS^{G12C}, yet show clearly decreased KRAS activation following SHP099 treatment. KRAS^{G12C} has significant intrinsic GTPase activity (18), as exemplified by covalent RAS inhibitors that target KRAS^{G12C}-GDP (34). Hence, even though KRAS^{G12C} is largely refractory to RAS-GAPs, significant conversion to RAS-GDP must occur in cells via this intrinsic GTPase activity, and ongoing GDP/GTP exchange is required to maintain steady-state levels of KRAS^{G12C}-GTP. Other RAS mutants (except Q61 alleles) also retain some intrinsic GTPase activity, although less than does KRAS^{G12C}. SHP099 also led to decreased pERK levels in RAS-less MEFs expressing KRAS^{G12D} and KRAS^{G12V} in a manner linearly related to residual KRAS-GTPase activity. Recently, Nichols and colleagues (35) also reported variable effects of a new allosteric SHP2 inhibitor on mutant KRAS, although its chemical matter was not reported and its specificity was not established using drug-resistant mutants.

Genetic and biochemical analyses have firmly established that SHP2 acts upstream of RAS (10, 11), but whether it promotes exchange, inhibits GAP activity, or both has been controversial. Early work showed that SHP2, via its C-terminal tyrosine phosphorylation sites, can recruit GRB2/SOS (36, 37). A subsequent study reported diminished RAS exchange in lysates from cells expressing a GAB1 mutant that cannot bind SHP2 (38). However, multiple other reports claim that SHP2 antagonizes RAS-GAP by dephosphorylating its binding sites on RTKs or on SHP2-binding scaffolding adapters (39–41). Studies of *Drosophila* embryogenesis also argue for actions of the SHP2 ortholog, CSW, on the GAP binding sites in TORSO (42). Our findings, and those of Nichols and colleagues (35), show clearly that SHP2 acts

upstream of SOS, and SHP2 inhibition can be bypassed by activated SOS, although we cannot exclude additional effects on RAS-GAP.

Single-agent SHP099 had little effect on 2-D proliferation or colony formation by cancer cells, but it significantly affected some xenografts and the KPC GEMM. There are several potential, non–mutually exclusive explanations for this apparent discrepancy. First, tumors occupy a hypoxic, nutrient-challenged, and potentially growth factor–deficient microenvironment; under such conditions, SHP2 might be essential for proliferation. Second, SHP2 might affect stromal support functions (e.g., growth factor production by cancer-associated fibroblasts, tumor angiogenesis). Tumor vascularity was decreased in all SHP099-treated xenografts, although whether this reflects direct inhibition of tumor angiogenesis or indirect effects on the tumor, with secondary effects on vessels, remains unclear. Third, SHP2 might affect the antitumor immune response, at least in the GEMMs. Interestingly, SHP099 and the drug combination had greater inhibitory effects in syngeneic mice than in nude mice (data not shown).

Our results comport with, and extend, previous studies of the effects of SHP2 modulation on other ERK pathway inhibitors. Prahallad and colleagues (14) found that SHP2 depletion (via *PTPN11* shRNA or deletion) blocked adaptive resistance to the $BRAF^{V600E}$ inhibitor vemurafenib. They claimed that an SHP2 catalytic domain inhibitor (GS493) had similar effects, but that agent has off-target effects on tyrosine kinases (43). While this article was in revision, three independent groups reported that inhibition of SHP2 can sensitize *KRAS*-mutant or *KRAS*-amplified cancers to MEK inhibitors (44–46). Our results are in general agreement with their findings, although these reports used either the nonspecific SHP2 inhibitor GS493 (45), the earlier-generation MEKi AZD6244, which has a very short half-life *in vivo* and is not approved for cancer therapy (44), or mouse trametinib doses 4 times higher than the human MTD (45, 46). We show that SHP099 is "on-target" using drug-resistant SHP2 mutants and provide new evidence that combination therapy affects the tumor microenvironment (angiogenesis and stroma), can, at least in some models, promote differentiation of highly anaplastic tumor cells, and, when delivered for sufficient time, can prevent tumor regrowth after drug withdrawal. Taken together, all of these studies suggest that SHP2 inhibition might be a broadly applicable strategy to prevent or overcome adaptive resistance to kinase inhibition in a wide array of malignancies.

METHODS

Cell Lines and Reagents

Cells were maintained in 5% CO_2 at 37°C under the conditions described by the vendor or the source laboratory; details are available from C. Fedele or K.H. Tang upon request. Cells were tested at least every 3 months for *Mycoplasma* contamination by PCR (47) and genotyped by short tandem repeat analysis at IDEXX Bioresearch. See Supplementary Methods for details. SHP099 (HY-100388A) was purchased from MedChemExpress. Selumetinib-AZD6244 (S1008), UO126 (S1102), and trametinib (GSK1120212-S2673) were purchased from Selleckchem.

Plasmids, Retroviral and Lentiviral Production

Lentiviral and retroviral constructs were generated by standard methods (see Supplementary Methods). Viruses were produced by cotransfecting HEK293T cells with lentiviral or retroviral constructs and packaging vectors. Stable pools of infected cells were selected by using the appropriate antibiotic or by FACS for EGFP.

Cell Assays

Cell number was monitored by the PrestoBlue assay (Thermo Fisher). Potential drug synergy was determined by BLISS analysis as: $Y_{ab,P} = Y_a + Y_b - Y_aY_b$, where Y_a stands for the percentage inhibition of drug *a* and Y_b stands for the percentage inhibition of drug *b* (48). For colony assays, cells (100–500) were seeded in 6-well plates and, after 16 hours, treated with DMSO or the indicated drugs. Colonies were stained with crystal violet, visualized by using the Odyssey Imaging System (LI-COR) and quantified with the ImageJ Colony Area PlugIn (49). For details, see Supplementary Methods. Cell-cycle distribution was monitored by flow cytometry using 7-AAD and analyzed by ModFit LT software (Verity Software House). Apoptosis was quantified by using the PE Annexin V Apoptosis Detection Kit (BD Biosciences).

Biochemical Assays

RAS activity was assessed by GST-RBD pulldown, followed by immunoblotting with pan-RAS or RAS isoform–specific antibodies. Whole-cell lysates were resolved by SDS-PAGE, followed by transfer to Nylon membranes. Immunoblots were performed with the indicated primary antibodies, followed by IRDye-conjugated secondary antibodies and visualization by LI-COR. For details, see Supplementary Methods.

IHC

pERK (Cell Signaling, 4370), CD31 (Cell Signaling, D8V9E), cleaved caspase-3 (Cell Signaling, D3E9), and Ki67 (Spring Biosciences, SP6) staining was performed on paraffin sections. OCT frozen sections were used for SA-βgal staining. Hematoxylin and eosin, Masson Trichrome, and PAS/Alcian Blue staining were performed by the Experimental Pathology Shared Resource at Perlmutter Cancer Center (PCC).

Animal Experiments

All animal experiments were approved by the NYU Langone Institutional Animal Care and Use Committee. Pancreas and lung cell line xenografts were established by subcutaneous injection of 5×10^6 cells in 50% Matrigel (Corning) into nude mice (*nu/nu*, #088 Charles River) MDA-MB-468 xenografts were established by injecting 5×10^6 cells in 50% Matrigel into the right lower mammary pad. Ovarian PDXs were established by injecting 5×10^5 cells in 50% Matrigel into the right lower mammary pad of NSG mice (The Jackson Laboratory). KPC 1203 cells (1×10^5 in Matrigel) were implanted into the pancreata of syngeneic male mice. Single agents and drug combinations were administered, and tumor size and body weight were monitored. For details, see Supplementary Methods.

qRT-PCR

Total RNA was isolated by the Qiagen RNeasy kit. cDNA was generated by using the SuperScript IV First Strand Synthesis System (Invitrogen). qRT-PCR was performed with Fast SYBR Green Master Mix (Applied Biosystems), following the manufacturer's protocol, in 384-well format in C1000 Touch Thermal Cycler (Bio-Rad). Differential gene-expression analysis was performed with CFX Manager (Bio-Rad) and normalized to GAPDH expression. Primers used are listed in Supplementary Table S2.

Statistical Analysis

Data are expressed as mean ± standard deviation. Statistical significance was determined using Student *t* test, Mann–Whitney *U* test,

or one-way ANOVA. Statistical analyses were performed in Prism 7 (GraphPad Software). Significance was set at $P = 0.05$.

Disclosure of Potential Conflicts of Interest

B.G. Neel has ownership interest (including stock, patents, etc.) in Navire Pharma and is a consultant/advisory board member for the same. No potential conflicts of interest were disclosed by the other authors.

Authors' Contributions

Conception and design: C. Fedele, H. Ran, B.G. Neel, K.H. Tang
Development of methodology: C. Fedele, H. Ran, K.H. Tang
Acquisition of data (provided animals, acquired and managed patients, provided facilities, etc.): C. Fedele, B. Diskin, W. Wei, J. Jen, M.J. Geer, K. Araki, D.M. Simeone, K.H. Tang
Analysis and interpretation of data (e.g., statistical analysis, biostatistics, computational analysis): C. Fedele, H. Ran, J. Jen, M.J. Geer, U. Ozerdem, G. Miller, B.G. Neel, K.H. Tang
Writing, review, and/or revision of the manuscript: C. Fedele, U. Ozerdem, D.M. Simeone, B.G. Neel, K.H. Tang
Administrative, technical, or material support (i.e., reporting or organizing data, constructing databases): C. Fedele, H. Ran, K. Araki, K.H. Tang
Study supervision: C. Fedele, B.G. Neel, K.H. Tang
Other (review and interpretation of histopathology slides as a pathologist): U. Ozerdem

Acknowledgments

We thank Drs. Alec Kimmelman, Dafna Bar-Sagi, Douglas A. Levine, Gottfried E. Konecny, Robert Rottapel, and Kwok-Kin Wong for cell lines; Drs. Dafna Bar-Sagi, Jason Moffat, and David Root for plasmids; and the PCC Experimental Pathology and Precision Immunology shared resources for technical support. We also thank Dr. Toshiyuki Araki for advice and discussion on this project. This work was supported by R01CA49152 to B.G. Neel and R01CA131045 to D.M. Simeone. This work was supported by NIH Research Project Grant Program R01 CA49152 and CA131045.

Received April 23, 2018; revised July 16, 2018; accepted July 23, 2018; published first July 25, 2018.

REFERENCES

1. Kandoth C, McLellan MD, Vandin F, Ye K, Niu B, Lu C, et al. Mutational landscape and significance across 12 major cancer types. Nature 2013;502:333–9.
2. Ciriello G, Miller ML, Aksoy BA, Senbabaoglu Y, Schultz N, Sander C. Emerging landscape of oncogenic signatures across human cancers. Nat Genet 2013;45:1127–33.
3. Zehir A, Benayed R, Shah RH, Syed A, Middha S, Kim HR, et al. Mutational landscape of metastatic cancer revealed from prospective clinical sequencing of 10,000 patients. Nat Med 2017;23:703–13.
4. Caunt CJ, Sale MJ, Smith PD, Cook SJ. MEK1 and MEK2 inhibitors and cancer therapy: the long and winding road. Nat Rev Cancer 2015;15:577–92.
5. Manchado E, Weissmueller S, Morris JPt, Chen CC, Wullenkord R, Lujambio A, et al. A combinatorial strategy for treating KRAS-mutant lung cancer. Nature 2016;534:647–51.
6. Sun C, Hobor S, Bertotti A, Zecchin D, Huang S, Galimi F, et al. Intrinsic resistance to MEK inhibition in KRAS mutant lung and colon cancer through transcriptional induction of ERBB3. Cell Rep 2014;7:86–93.
7. Anderson GR, Winter PS, Lin KH, Nussbaum DP, Cakir M, Stein EM, et al. A landscape of therapeutic cooperativity in KRAS mutant cancers reveals principles for controlling tumor evolution. Cell Rep 2017;20:999–1015.
8. Duncan JS, Whittle MC, Nakamura K, Abell AN, Midland AA, Zawistowski JS, et al. Dynamic reprogramming of the kinome in response to targeted MEK inhibition in triple-negative breast cancer. Cell 2012;149:307–21.
9. Zawistowski JS, Bevill SM, Goulet DR, Stuhlmiller TJ, Beltran AS, Olivares-Quintero JF, et al. Enhancer remodeling during adaptive bypass to MEK inhibition is attenuated by pharmacologic targeting of the P-TEFb complex. Cancer Discov 2017;7:302–21.
10. Ran H, Tsutsumi R, Araki T, Neel BG. Sticking it to cancer with molecular glue for SHP2. Cancer Cell 2016;30:194–6.
11. Chan G, Neel BG. Role of PTPN11 (SHP2) in Cancer. Protein Tyrosine Phosphatases in Cancer. New York: Springer; 2016. p115–43.
12. Chen YN, LaMarche MJ, Chan HM, Fekkes P, Garcia-Fortanet J, Acker MG, et al. Allosteric inhibition of SHP2 phosphatase inhibits cancers driven by receptor tyrosine kinases. Nature 2016;535:148–52.
13. Garcia Fortanet J, Chen CH, Chen YN, Chen Z, Deng Z, Firestone B, et al. Allosteric inhibition of SHP2: identification of a potent, selective, and orally efficacious phosphatase inhibitor. J Med Chem 2016;59:7773–82.
14. Prahallad A, Sun C, Huang S, Di Nicolantonio F, Salazar R, Zecchin D, et al. Unresponsiveness of colon cancer to BRAF(V600E) inhibition through feedback activation of EGFR. Nature 2012;483:100–3.
15. Hingorani SR, Wang L, Multani AS, Combs C, Deramaudt TB, Hruban RH, et al. Trp53R172H and KrasG12D cooperate to promote chromosomal instability and widely metastatic pancreatic ductal adenocarcinoma in mice. Cancer Cell 2005;7:469–83.
16. Moore PS, Sipos B, Orlandini S, Sorio C, Real FX, Lemoine NR, et al. Genetic profile of 22 pancreatic carcinoma cell lines. Analysis of K-ras, p53, p16 and DPC4/Smad4. Virchows Arch 2001;439:798–802.
17. Sun C, Yamato T, Furukawa T, Ohnishi Y, Kijima H, Horii A. Characterization of the mutations of the K-ras, p53, p16, and SMAD4 genes in 15 human pancreatic cancer cell lines. Oncol Rep 2001;8:89–92.
18. Hunter JC, Manandhar A, Carrasco MA, Gurbani D, Gondi S, Westover KD. Biochemical and structural analysis of common cancer-associated KRAS mutations. Mol Cancer Res 2015;13:1325–35.
19. Drosten M, Dhawahir A, Sum EY, Urosevic J, Lechuga CG, Esteban LM, et al. Genetic analysis of Ras signalling pathways in cell proliferation, migration and survival. EMBO J 2010;29:1091–104.
20. Patgiri A, Yadav KK, Arora PS, Bar-Sagi D. An orthosteric inhibitor of the Ras-Sos interaction. Nat Chem Biol 2011;7:585–7.
21. Pratilas CA, Taylor BS, Ye Q, Viale A, Sander C, Solit DB, et al. (V600E)BRAF is associated with disabled feedback inhibition of RAF-MEK signaling and elevated transcriptional output of the pathway. Proc Natl Acad Sci U S A 2009;106:4519–24.
22. Gilmartin AG, Bleam MR, Groy A, Moss KG, Minthorn EA, Kulkarni SG, et al. GSK1120212 (JTP-74057) is an inhibitor of MEK activity and activation with favorable pharmacokinetic properties for sustained *in vivo* pathway inhibition. Clin Cancer Res 2011;17:989–1000.
23. Yao Z, Yaeger R, Rodrik-Outmezguine VS, Tao A, Torres NM, Chang MT, et al. Tumours with class 3 BRAF mutants are sensitive to the inhibition of activated RAS. Nature 2017;548:234–8.
24. Lin L, Sabnis AJ, Chan E, Olivas V, Cade L, Pazarentzos E, et al. The Hippo effector YAP promotes resistance to RAF- and MEK-targeted cancer therapies. Nat Genet 2015;47:250–6.
25. Xue Y, Martelotto L, Baslan T, Vides A, Solomon M, Mai TT, et al. An approach to suppress the evolution of resistance in BRAF(V600E)-mutant cancer. Nat Med 2017;23:929–37.
26. Nair AB, Jacob S. A simple practice guide for dose conversion between animals and human. J Basic Clin Pharm 2016;7:27–31.
27. Eisenhauer EA, Therasse P, Bogaerts J, Schwartz LH, Sargent D, Ford R, et al. New response evaluation criteria in solid tumours: revised RECIST guideline (version 1.1). Eur J Cancer 2009;45:228–47.
28. Cancer Genome Atlas Network. Comprehensive molecular portraits of human breast tumours. Nature 2012;490:61–70.
29. Cancer Genome Atlas Research Network. Integrated genomic analyses of ovarian carcinoma. Nature 2011;474:609–15.

30. Marcotte R, Sayad A, Brown KR, Sanchez-Garcia F, Reimand J, Haider M, et al. Functional genomic landscape of human breast cancer drivers, vulnerabilities, and resistance. Cell 2016;164:293–309.
31. Marcotte R, Brown KR, Suarez F, Sayad A, Karamboulas K, Krzyzanowski PM, et al. Essential gene profiles in breast, pancreatic, and ovarian cancer cells. Cancer Discov 2012;2:172–89.
32. Nazarian R, Shi H, Wang Q, Kong X, Koya RC, Lee H, et al. Melanomas acquire resistance to B-RAF(V600E) inhibition by RTK or N-RAS upregulation. Nature 2010;468:973–7.
33. Fulcher LJ, Hutchinson LD, Macartney TJ, Turnbull C, Sapkota GP. Targeting endogenous proteins for degradation through the affinity-directed protein missile system. Open Biol 2017;7:pii:170066.
34. Dang CV, Reddy EP, Shokat KM, Soucek L. Drugging the 'undruggable' cancer targets. Nat Rev Cancer 2017;17:502–8.
35. Nichols RJ, Haderk F, Stahlhut C, Schulze CJ, Hemmati G, Wildes D, et al. Efficacy of SHP2 phosphatase inhibition in cancers with nucleotide-cycling oncogenic RAS, RAS-GTP dependent oncogenic BRAF and NF1 loss. bioRxiv 2017.
36. Bennett AM, Tang TL, Sugimoto S, Walsh CT, Neel BG. Protein-tyrosine-phosphatase SHPTP2 couples platelet-derived growth factor receptor beta to Ras. Proc Natl Acad Sci U S A 1994;91:7335–9.
37. Li W, Nishimura R, Kashishian A, Batzer AG, Kim WJ, Cooper JA, et al. A new function for a phosphotyrosine phosphatase: linking GRB2-Sos to a receptor tyrosine kinase. Mol Cell Biol 1994;14:509–17.
38. Yamasaki S, Nishida K, Yoshida Y, Itoh M, Hibi M, Hirano T. Gab1 is required for EGF receptor signaling and the transformation by activated ErbB2. Oncogene 2003;22:1546–56.
39. Agazie YM, Hayman MJ. Molecular mechanism for a role of SHP2 in epidermal growth factor receptor signaling. Mol Cell Biol 2003;23:7875–86.
40. Montagner A, Yart A, Dance M, Perret B, Salles JP, Raynal P. A novel role for Gab1 and SHP2 in epidermal growth factor-induced Ras activation. J Biol Chem 2005;280:5350–60.
41. Fambrough D, McClure K, Kazlauskas A, Lander ES. Diverse signaling pathways activated by growth factor receptors induce broadly overlapping, rather than independent, sets of genes. Cell 1999;97:727–41.
42. Cleghon V, Feldmann P, Ghiglione C, Copeland TD, Perrimon N, Hughes DA, et al. Opposing actions of CSW and RasGAP modulate the strength of Torso RTK signaling in the Drosophila terminal pathway. Mol Cell 1998;2:719–27.
43. Tsutsumi R, Ran H, Neel BG. Off-target inhibition by active site-targeting SHP2 inhibitors. FEBS Open Bio 2018;8:1405–11.
44. Mainardi S, Mulero-Sánchez A, Prahallad A, Germano G, Bosma A, Krimpenfort P, et al. SHP2 is required for growth of KRAS-mutant non-small-cell lung cancer in vivo. Nat Med 2018;24:961–7.
45. Ruess DA, Heynen GJ, Ciecielski KJ, Ai J, Berninger A, Kabacaoglu D, et al. Mutant KRAS-driven cancers depend on PTPN11/SHP2 phosphatase. Nat Med 2018;24:954–60.
46. Wong GS, Zhou J, Liu JB, Wu Z, Xu X, Li T, et al. Targeting wild-type KRAS-amplified gastroesophageal cancer through combined MEK and SHP2 inhibition. Nat Med 2018;24:968–77.
47. Young L, Sung J, Stacey G, Masters JR. Detection of Mycoplasma in cell cultures. Nat Protoc 2010;5:929–34.
48. Zhao W, Sachsenmeier K, Zhang L, Sult E, Hollingsworth RE, Yang H. A new bliss independence model to analyze drug combination data. J Biomol Screen 2014;19:817–21.
49. Guzman C, Bagga M, Kaur A, Westermarck J, Abankwa D. ColonyArea: an ImageJ plugin to automatically quantify colony formation in clonogenic assays. PLoS One 2014;9:e92444.